Computational Biology and Chemistry 89 (2020) 107378

Contents lists available at ScienceDirect

Computational Biology and Chemistry

journal homepage: www.elsevier.com/locate/cbac

Research Article

New naphthalene derivative for cost-effective AChE inhibitors for Alzheimer's treatment: *In silico* identification, *in vitro* and *in vivo* validation

Fareeha Anwar [a], Uzma Saleem [b], Bashir Ahmad [a], Muhammad Ashraf [c], Atta Ur Rehman [d], Matheus Froeyen [e], Lee Yean Kee [f], Iskandar Abdullah [f], Muhammad Usman Mirza [e], Sarfraz Ahmad [f,*]

[a] Riphah Institute of Pharmaceutical Sciences, Riphah International University, Lahore, Pakistan
[b] Faculty of Pharmaceutical Sciences, GC University, Faisalabad 38000, Pakistan
[c] Department of Chemistry, The Islamia University of Bahawalpur, Bahawalpur 63100, Pakistan
[d] Department of Pharmacy, Forman Christian University, Lahore 54600, Pakistan
[e] Department of Pharmaceutical and Pharmacological Sciences, Rega Institute for Medical Research, Medicinal Chemistry, University of Leuven, B-3000 Leuven, Belgium
[f] Drug Design and Development Research Group (DDDRG), Department of Chemistry, Faculty of Science, University of Malaya, Kuala Lumpur 50603, Malaysia

ARTICLE INFO

Keywords:
Acetylcholinesterase
Butyrylcholinesterase
Lipoxygenase
α-Glucosidase
DPPH

ABSTRACT

Neurodegenerative diseases have complex etiology and pose a challenge to scientists to develop simple and cost-effective synthetic compounds as potential drug candidates for such diseases. Here, we report an extension of our previously published *in silico* screening, where we selected four new compounds as AChE inhibitors. Further, based on favorable binding possess, MD simulation and MMGBSA, two most promising compounds (**3a** and **3b**) were selected, keeping in view the ease of synthesis and cost-effectiveness. Due to the critical role of BChE, LOX and α-glucosidase in neurodegeneration, the selected compounds were also screened against these enzymes.

The IC_{50} values of **3a** against AChE and BChE found to be 12.53 and 352.42 μM, respectively. Moderate to slight inhibitions of 45.26 % and 28.68 % were presented by **3a** against LOX and α-glucosidase, respectively, at 0.5 mM. Insignificant inhibitions were observed with **3b** against the four selected enzymes. Further, *in vivo* trial demonstrated that **3a** could significantly diminish AChE levels in the mice brain as compared to the control. These findings were in agreement with the histopathological analysis of the brain tissues. The results corroborate that selected compounds could serve as a potential lead for further development and optimization as AChE inhibitors to achieve cost-effective anti-Alzheimer's drugs.

1. Introduction

Slow and gradual mental deterioration and diminution in cognition is a customary part of the aging process. In some people, it becomes relatively accelerated with respect to aging, which results in impairment of everyday life functions. It is believed to be a syndrome called dementia and is associated with numerous other symptoms, most commonly including decreased motivation, difficulty in language and emotional problems. Complete underlying causes of this phenomenon are not clear, but the most significant cause in its progression includes genetics, along with the role of environment and lifestyle. Around 50 million people worldwide have dementia, with the introduction of about 10 million new cases every year (World Health Organization, 2019).

The most common form of dementia is Alzheimer's disease (AD), which accounts for 60–70% of cases (World Health Organization, 2019). Studies revealed that it occurs after the age of 65 years, but an increase in socioeconomic and social life burdens shorten the age for dementia (Qiu et al., 2009). It has been suggested that its pathogenesis is based on three hypotheses; (1) cholinergic, (2) amyloid, and (3) tau hypothesis (Hebert et al., 2003; Crespo-Biel et al., 2012). Among these hypotheses, the dysfunction of the acetylcholine system is the key etiology of the AD.

On therapeutic fronts, acetylcholinesterase (AChE) inhibitors open a new era for the AD treatment. Up till now, different AChE inhibitors (donepezil, tacrine, galantamine, rivastigmine, *etc.*) have been approved by the FDA and used as a frontline treatment for AD (Piazzi et al., 2008). A complete cure of AD is not available, and these drugs are used to mitigate various associated symptoms and retardation of the memory loss and disease development. The clinical efficacy of the available drugs

* Corresponding author.
E-mail address: sarfraz.ahmad@um.edu.my (S. Ahmad).

https://doi.org/10.1016/j.compbiolchem.2020.107378
Received 23 July 2020; Received in revised form 16 August 2020; Accepted 15 September 2020
Available online 18 September 2020

remains a question and usually have been proved to pose little to no effect. Another major challenge in AD treatment is a long-term medication which raises a substantial fiscal load on healthcare institutes. So there is a dire need of the new agents with improved efficacy and low cost (Dickson and Gagnon, 2009).

Lipoxygenases (LOXs) are enzymes that catalyze lipid hydroperoxidation and regulate chronic inflammation (Di Francesco et al., 2013). A growing body of evidence suggests that 5-lipoxygenase (5-LOX) and its corresponding leukotrienes have a strong involvement in brain inflammation related to the prognosis of neurodegeneration and age-dependent dementia (Sugaya et al., 2000; Rådmark et al., 2007). The inhibition of 5-LOX could serve as a safe anti-inflammatory approach for the control of AD-associated neurodegeneration (Di Francesco et al., 2013).

Impaired uptake and metabolism of glucose is a hallmark and primary aetiology concomitant with AD, initiated many years before the disease becomes symptomatic, particularly in sporadic AD (Cao et al., 2003). Reduction in glucose consumption ranges from 10 to 40 % depending upon the severity of the disease (Jia et al., 2017). On the other hand, diabetes mellitus is the provoking cause of dementia. Insulin controls the synaptic and cholinergic functions in the brain. The decrease in insulin levels in the brain causes the neurodegeneration that leads to the loss of cholinergic transmission (De Felice and Ferreira, 2014).

Moreover, glucose imbalance and raised amount of lipids in AD brain upregulate lipid peroxidation giving rise to disturbed redox homeostasis and oxidative stress (Rojas-Gutierrez et al., 2017). This situation can promote neurodegeneration by damaging intracellular contents (Polidori and Mecocci, 2002). Besides, the impairment of insulin signaling has previously been linked with raised mitochondrial dysfunction and oxidative stress in neurons (Hoyer and Lannert, 1999). Accumulation of reactive oxygen species (ROS) in AD patients induces mitochondrial damage and promotes the production of β-amyloid plaques and neurofibrillary tangles, leading to the development of AD (Matsuoka et al., 2001).

In the present era, *in silico* studies have greatly facilitated the selection of promising compounds for bench investigations (Ikram et al., 2019; Noor et al., 2019; Saleem et al., 2019). The design of the current project is based on the study of *in silico* acetylcholinesterase inhibitors for their potential role against AD (Iman et al., 2018). Apart from acetylcholinesterase, due to the role of butyrylcholinesterase, inflammation, oxidative stress and glucose uptake in AD, the selected compounds were also tested against LOX, di(phenyl)-(2,4,6-trinitrophenyl) iminoazanium (DPPH) and α-Glu.

Naphthalene structure has been proven to be an efficient platform for the synthesis of new compounds that may have various biological and clinical applications. Many naphthalene derivatives have been identified as a new potent antimicrobial, antihypertensive, antimalarial and antitubulin. Several naphthalene based drugs such as nafcillin, terbinafine and naftifine are armamentarium of the therapeutics being used presently (Desai et al., 2012). The present study deals with the computer-aided discovery of naphthalene-based AChE inhibitors, and there *in vitro* and *in vivo* evaluations as anti-AD leads. Alongside this, selected compounds have also been evaluated for their inhibitory potential against BChE, LOX, and α-glucosidase.

2. Material and methods

2.1. Materials

2-Naphthol, 3,5-dinitrobenzoic acid, 2-chloro-5-nitrobenzoic acid, triethylamine and related chemicals and solvents used were of analytical grade and purchased from the local supplier of Sigma Aldrich (St. Louis, MO, USA).

2.2. Synthesis

The general reaction scheme followed for the synthesis of selected naphthalen-2-yl 3,5-dinitrobenzoate (**3a**) and naphthalen-2-yl 2-chloro-5-nitrobenzoate (**3b**) is presented in Fig. 1.

2.2.1. General procedure for the synthesis of acid chlorides (2)

Carboxylic acid (**1**) (5 mmol) and phosphorus pentachloride (1.5 eq., 1.56 g, 7.5 mmol) were mixed in dry toluene (100 ml), calcium chloride drying tube was applied at the top of the condenser and the reaction mixture was refluxed for 1.5 h. The completion of the reaction was confirmed by TLC and the solvent was evaporated on a rotary evaporator. The resulting product was pure enough for further reaction.

2.2.2. General procedure for the synthesis of esters (3)

Acid chloride (**2**) was dissolved in dry chloroform and cooled on an ice bath under nitrogen atmosphere. A solution of 2-naphthol (0.85 eq.) in dry chloroform was added to the solution of acid chloride in dry chloroform on ice bath along with stirring. Dry triethylamine (1 eq.) was added to the reaction mixture, the ice bath was removed, and the reaction mixture was stirred overnight under nitrogen atmosphere. The reaction mixture was shifted to the separating funnel, 150 mL chloroform was added, and the organic layer was washed twice with 1 N NaOH and water until the water phase reacted neutral. Sodium sulphate was added to the organic phase, filtered and the solvent evaporated on a rotary evaporator. The product was crystallized from ethanol and dried in the desecrator to get analytically pure product.

Yields, melting points and spectral data are provided in supporting information.

2.3. In vitro assay

2.3.1. AChE & BChE assays

Acetylcholine esterase and butyrylcholine esterase activities were measured by using the Ellman's method. The reaction mixture consisted of 160 µL of tris HCl buffer (50 mM, pH 7.4), 10 µL of the enzyme (0.005 unit/well for AChE or 0.5 unit/well for BChE) in their respective wells. Mixtures were mixed well and incubated for 10 min at 25℃. After incubation, the absorbance was recorded at 412 nm. The reaction was initiated by the addition of 10 µL DTNB (1 mM) solution and 20 µL substrate (acetylthiocholine iodide (3 mM) for AChE and butyrylthiocholine chloride (0.5 mM) for BChE). The reaction mixture was incubated for 15 min at room temperature and absorbance was recorded at 412 nm. In control, the enzyme was added after the DTNB reagent (Yar et al., 2014a). Eserine was used as a standard and the experiment was carried out in triplicate. IC_{50} values were calculated using the EZ-Fit enzyme kinetics software (Perrella Scientific Inc. Amherst USA).

2.3.2. Lipoxygenase assay

For the LOX assay, the reaction mixture contained 140 µL of sodium phosphate buffer (100 mM, pH 8.0), 20 µL of test compound and 15 µL of purified LOX enzyme (600 U). The plate was read at 234 nm and the reaction mixture was incubated at 25℃ for 10 min. The reaction was initiated by the addition of 25 µL of the substrate (linoleic acid in tween 20). The change in absorbance was measured at 234 nm after 6 min of reaction. Quercetin was used as a standard and experiment was performed in triplicate and percentage inhibition was calculated by using the following formula (Yar et al., 2014b).

$$Inhibition\ (\%) = \frac{Abs.\ of\ control - Abs.\ of\ test}{Abs.\ of\ Control} \times 100$$

2.3.3. α-Glucosidase assay

In a total reaction mixture contained 70 µL phosphate buffer (50 mM, pH 6.8), 10 µL (0.5 mM) test compound and 10 µL of the α-Glu enzyme. Before the incubation reaction mixture was pre-read at 400 nm. The

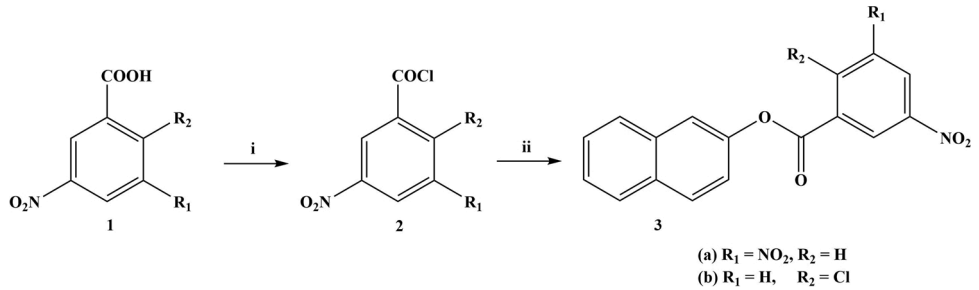

Fig. 1. General synthesis scheme for naphthalen-2-yl 3,5-dinitrobenzoate (**3a**) and naphthalen-2-yl 2-chloro-5-nitrobenzoate (**3b**); (i) dry toluene, PCl_5, reflux, 1.5 h, (ii) dry chloroform, 2-naphthol, 0 °C, triethylamine, rt overnight.

reaction mixture was incubated at 37℃ for 10 min and the reaction was initiated by the addition of 10 µL of the substrate (0.5 mM, p-nitrophenyl glucopyranoside). The reaction mixture was incubated for 30 min at 37℃ and absorbance was measured at 400 nm (Riaz et al., 2015). Acarbose was used as a standard and percentage inhibition was measured by using the same formula described in LOX assay.

2.3.4. DPPH free radical scavenging assay

The selected concentration of test sample or standard rutin (1 mL) (0.125, 0.25, 0.5, 1 and 2 mg/ml in methanol) was mixed with 3 mL DPPH (0.01 mM in methanol) and the reaction mixture was incubated at room temperature for 1 h in the dark. Absorbance was read at 515 nm (Kang and Saltveit, 2002). The percentage antioxidant activity (%AA) was measured by using the following formula:

$$AA\% = 100 - \frac{(Abs\ control - Abs\ sample) \times 100}{Abs\ control}$$

2.4. In vivo assay

Swiss albino mice of either sex, weighing 30−35 g, 6–8 weeks old were selected for this study. All the experimental animals were placed in controlled conditions like 22 ± 2℃ temperature, 45–55 % humidity and 12 h light and dark cycle and provided with standard animal diet and water. Before the commencement of the study, permission was taken from the research ethical committee of Riphah international university with a voucher number of REC/RIPS-LHR/2020/033. This committee followed the rules and regulations of the Institute of Laboratory Animals Resources, Commission on Life Sciences University, National Research Council (1996).

2.4.1. Study design

The male and female animals were randomly divided into three groups having six subjects in each group (n = 6). Group I served as negative control and received vehicle (carboxymethyl cellulose, 1 mL/kg) while group II and III received 5 mg/kg dose of **3a** and **3b**, respectively. All the treatments were given *via* oral route for one week once daily.

2.4.2. Acetylcholinesterase assay

After the treatment, animals were anesthetized with 3–5 % isoflurane diluted with oxygen and then sacrificed by cervical dislocation method. The brain was removed and homogenized with phosphate buffer (pH 7.4). The supernatant was removed after centrifugation at 4000 rpm for 10 min at 4℃. In 0.4 mL homogenate, 2.6 mL phosphate buffer (pH 8) and 100 µL of DTNB reagent were added. Initial absorbance was noted at 412 nm and then 20 µL of acetyl thiocholine iodide (substrate) was added in the reaction mixture and change in absorbance was measured for ten minutes.

Mean change in absorbance was obtained and the rate of the mole of acetylthiocholine iodide hydrolyzed/min/gm of brain tissue (R) was calculated by using formula $R = 5.74 \times 10^{-4} \times A/Co$. Where, A is mean change in absorbance per minute and Co is original concentration (Hira et al., 2019).

2.4.3. Histopathological analysis

After sacrificing the brain was removed and preserved in a 10 % formalin solution. After the tissue fixation in a paraffin block, the sections were cut using a digital microtome and histological analysis was performed using the hematoxylin and eosin staining.

2.5. Molecular docking studies

The corresponding proteins were retrieved from the Protein databank. These include human acetylcholinesterase bound with huprine W (PDB ID: 4BDT) and human butyrylcholinesterase (PDB ID: 4BDS) complexed with tacrine. The proteins were prepared, optimized and minimized prior to docking as explained in previous studies (Iman et al., 2018; Mirza et al., 2019). Briefly, heteroatoms were removed, while hydrogens and charges were added followed by energy minimization using AMBER ff14SB force field (Maier et al., 2015). The ligands were prepared, minimized and saved to MOL2 format. Molecular docking was performed using AutoDock Vina (Trott and Olson, 2010) which uses a gradient optimization method that approximates the ligand-binding affinity in kcal/mol and ranks the best poses efficiently. Individual ligands were docked into the respective active sites of the representative structures. The (x,y,z) coordinates for the gird-centers of AChE and BChE were (-1.93,-36.44,-51.87) and (135.31,115.98,42.05), respectively. The cubical grids with 25 Å length were used.

2.5.1. MMGBSA binding free energy calculations

To estimate the total binding free energies, molecular dynamics (MD) simulations were performed (AMBER18 simulation package) using the explicit solvent environment (TIP3 molecule system) in the octahedral box (10A dimensions from solute) under standard temperature (300 K) and pressure (1 bar) for a period of 20 ns. We employed the same MD protocol as implemented in other related studies (Iman et al., 2018; Mirza et al., 2019, 2016). The MD simulated most representative conformation was extracted from each simulation system in PDB format and analyzed from molecular interactions. The binding free energies (ΔG_{tol}) of representative docked complexes were calculated using the MMGBSA method (Hou et al., 2011a), implemented in AMBER 18. A total of 1000 snapshots with an interval of 2 ps (picosecond) were generated from 20 ns MD simulation and binding energy is calculated as follows:

$$\Delta E_{elec} = \Delta E_{int} + \Delta E_{ele} + \Delta E_{vdw}$$

$$\Delta G_{sol} = \Delta G_{p} + \Delta G_{np}$$

$$\Delta G_{bind}\ (\Delta G_{pred}) = \Delta E_{MM} + \Delta G_{sol} - T\Delta S$$

(ΔE_{MM}) is molecular mechanics binding energy which is further divided into internal energy (ΔE_{int}), electrostatic energy (ΔE_{ele}), and van der Waals energy (ΔE_{vdw}); total solvation free energy (ΔG_{sol}) is

contributed by the sum of polar (ΔG_p) and non-polar (ΔG_{np}) components; -TΔS is the change of conformational entropy upon ligand binding. The later entropic calculations are computationally expensive and give better accuracy (Hou et al., 2011b). The performance of the MMGBSA method has already been well-documented previously (Hou et al., 2011a, b; Genheden and Ryde, 2015; Sun et al., 2014; Xu et al., 2013).

The experimental binding energies (ΔG_{exp}) were calculated from IC_{50} by the following equation, using the gas (R) and temperature (T) constant and compared with ΔG_{exp}.

$$\Delta Gexp = RT \ln IC_{50}$$

3. Results

3.1. In vitro assay

Results revealed that **3a** depicted a promising potential of 89.13 % inhibition against AChE in *in vitro* along with the moderate activities against BChE (63.27 %), LOX (45.26 %) and α-Glu (28.68 %) at 0.5 mM concentration. The compound **3b** showed around 35 % inhibition of AChE, LOX and α-Glu and a very low inhibition of 21.68 % against BChE at 0.5 mM concentration (Table 1).

Due to the promising potential against AChE, **3a** was further evaluated for IC_{50} value against AChE and BChE, producing 50 % inhibition of enzymes at 12.53 ± 0.21 and 325.42 ± 5.3 μM, respectively (Table 1). The experiments were repeated in triplicate and the values represent mean and standard deviation.

3.2. DPPH free radical scavenging assay

The selected naphthalene derivatives did not show any promising free radical scavenging activity when compared with rutin at different concentration levels (Table 2). Five different concentrations ranging from 0.125 to 2 mg/ml were tested against DPPH and maximum inhibition of around 20 % was observed at 2 mg/ml in the case of **3a**, while standard rutin presented 82.74 % inhibition at this concentration.

3.3. In vivo acetylcholinesterase assay

In vivo acetylcholinesterase assay revealed that **3a** and **3b** significantly decreased AChE levels in the brain tissues compared with the control group. The results are presented in Fig. 2. The values are represented as mean and standard deviation of six readings.

3.3.1. Histopathological analysis

Histopathological studies showed the normal architecture and intact cells present in the slide sections in all treatment groups (Fig. 3).

Table 1
In vitro percentage inhibition of selected compounds (**3a** and **3b**) and their respective standards against AChE, BChE, LOX and α-Glu enzymes.

Enzymes	% Inhibition at 0.5 mM			IC_{50} (μM)
	Standard	3a	3b	3a
AChE	91.46 ± 1.25	89.13 ± 0.57	35.29 ± 0.36	12.53 ± 0.21
BChE	83.75 ± 1.16	63.27 ± 0.75	21.68 ± 0.45	325.42 ± 5.3
LOX	89.25 ± 0.62	45.26 ± 0.56	35.37 ± 0.58	–
α-Glu	65.73 ± 1.93	28.68 ± 1.20	35.65 ± 1.74	–

Eserine was used as a standard for AChE and BChE assay while quercetin and acarbose were used as standards for LOX and α-Glu, respectively. Data represented as mean ± standard deviation, n = 3.

Table 2
Percentage DPPH radical scavenging potentials of standard rutin and test compounds (**3a** and **3b**) at 0.125, 0.25, 0.5, 1 and 2 mg/mL.

Concentration (mg/mL)	Percentage DPPH scavenging activity		
	Rutin	3a	3b
2	82.74 ± 0.831	20.44 ± 0.63	6.5 ± 0.12
1	73.78 ± 1.109	15.80 ± 0.35	5.40 ± 0.24
0.5	68.51 ± 1.599	14.84 ± 0.20	4.7 ± 1.2
0.25	56.59 ± 1.787	9.76 ± 0.03	4.6 ± 3.2
0.125	43.42 ± 1.033	5.67 ± 0.197	3.1 ± 0.58

The data represented as the mean ± standard deviation with n = 3.

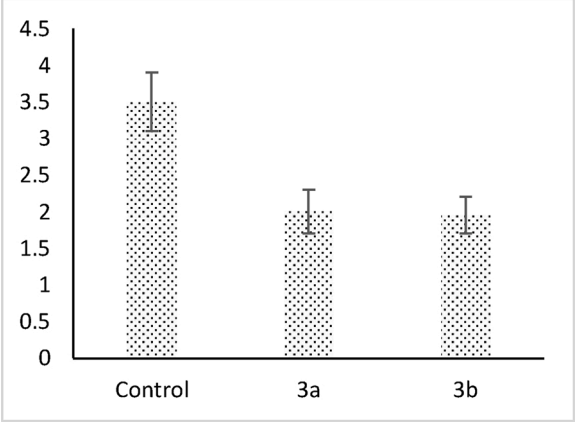

Fig. 2. AChE levels (μmole/min/mg of protein) in brain tissues of control, **3a** and **3b** groups.

3.4. Molecular modeling studies

Molecular docking studies were performed to analyze the predicted binding poses of corresponding compounds with thee crystal structure of AChE and BChE and plausible binding free energy was estimated after 20 ns MD simulation in the explicit solvent under standard temperature and pressure.

3.4.1. Predicted binding mode of compounds against AChE and BChE enzymes

The complexes were simulated for a period of 20 ns and potential binding poses of the compounds were investigated. Both compounds (**3a** and **3b**) were found to remain deep inside the gorge and showed overall ligand RMSD less than 1 Å, which validates the stability of ligand inside the active site (Figs. 4 and 5). More in-depth molecular interaction analysis shown in Fig. 4 revealed that the dinitrobenzene moiety of **3a** established three H-bonds with the side chains of Tyr341 and Thr83. This network of H-bonds anchored the terminal dinitrobenzene moiety to establish strong π-π interaction with Tyr337 and Trp86. Moreover, the oxygen atom connected to naphthalene also formed one H-bond with Tyr337. Likewise, **3b** also established π-π interaction with Tyr337 and Trp86 with two additional H-bonds formed by the oxygen atom connected to naphthalene with Tyr337 and terminal nitrobenzene with Ser125. Previous studies have reported that Tyr72 and Trp286, and Trp86 residues play a vital role in AChE inhibition.

Both compounds showed consensus binding mode with strong π-π interaction with aromatic residues Tyr337 and Trp86, but compound **3a** was found to be the most potent (89.13 % inhibition) as compared to the **3b** (35.29 % inhibition). Although **3a** and **3b** have the naphthalene moiety, which slightly contributed, **3a** has two strong electron-withdrawing nitro groups on the terminal benzene ring. The presence of these two nitro groups might play an important role in AChE inhibition, which formed three H-bonds with Tyr341 and Thr83 addition to

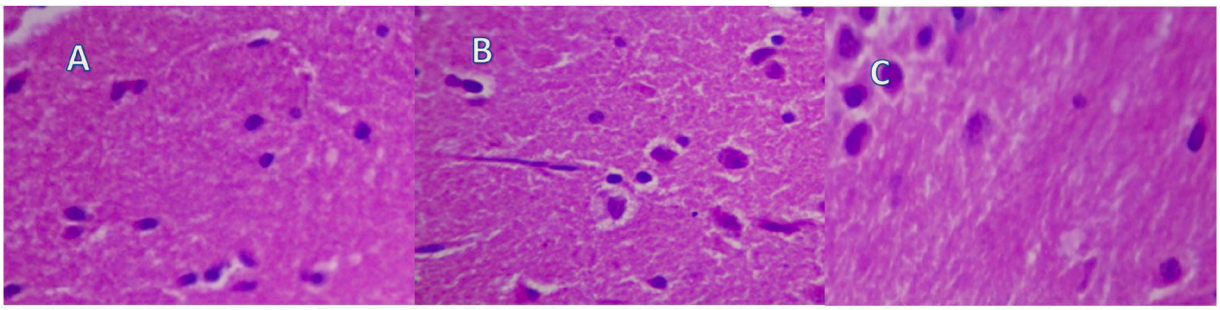

Fig. 3. Histopathology of normal control (A), **3a** (B) and **3b** (C).

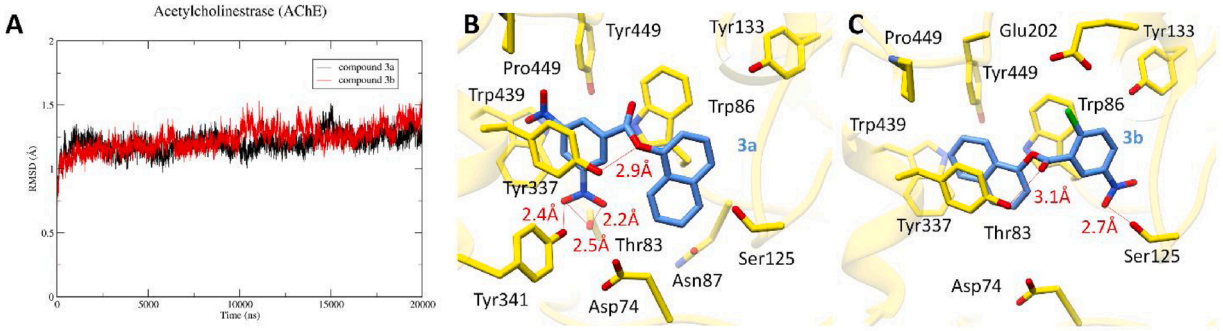

Fig. 4. (A) Root-mean-square-deviation of AChE complexed with compound 3a (black) and 3b (red) over a period of 20 ns. Both complexes showed all-atom backbone stability as depicted by MD simulation of conformations of **3a (B)** and **3b (C)** inside the binding pocket of AChE. Molecular interactions of individual compounds are displayed, and residues are labelled accordingly.

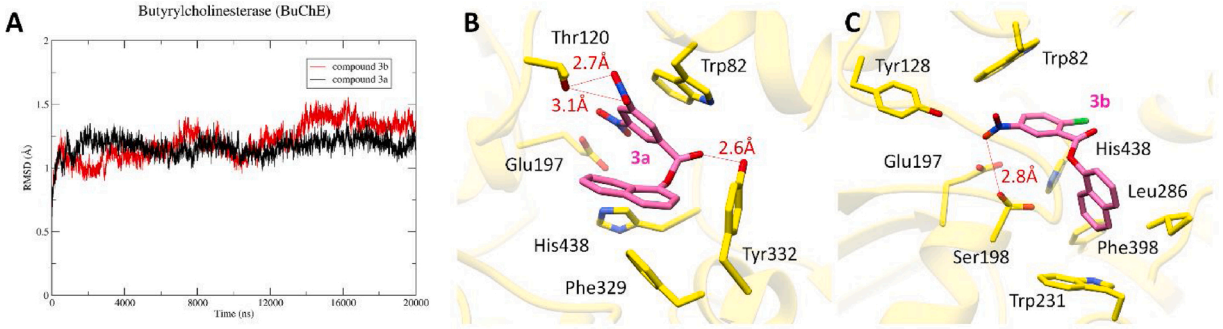

Fig. 5. (A) Root-mean-square-deviation of BChE complexed with compound 3a (black) and 3b (red) over a period of 20 ns. Both complexes showed all-atom backbone stability in MD simulation of conformations of **3a (B)** and **3b (C)** inside the binding pocket of BChE. Molecular interactions of individual compounds are displayed, and residues are labelled accordingly.

stalking interactions. In BChE complexes, **3b** established one H-bond between the terminal nitro group and Ser198, where dinitrobenzene moiety of **3a** established strong π-π interaction with Trp82 and formed two H-bonds with the side chain of Thr120. Like AChE inhibition, the presence of two nitro groups in the terminal region of **3a** might play an important role in BChE inhibition (Fig. 5).

3.4.2. *Predicted free energy of binding (ΔG_{bind})*

To evaluate the contribution of molecular mechanics and solvation energies, absolute ligand's free energy of binding was evaluated with the

Table 3
Molecular mechanics generalized born surface area (MMGBSA) binding free energy calculation of the **3a** and **3b** against AChE and BChE.

Targets	Cpds	ΔE_{vdw}	ΔE_{ele}	ΔE_{MM}	ΔG_p	ΔG_{np}	ΔG_{sol}	ΔG_{tol}	-TΔS	ΔG_{bind} (ΔG_{pred})	Ki_{cal} (nM)
AChE	**3a**	−42.11	−16.2	−58.31	29.65	−5.77	23.88	−34.43	20.3	−14.13	0.051
	3b	−40.26	−9.14	−49.4	28.12	−5.14	22.98	−26.42	18.1	−8.32	868.98
BChE	**3a**	−39.88	−14.21	−54.09	29.41	−6.77	22.64	−31.45	20.12	−11.33	5.575
	3b	−37.19	−8.15	−45.34	28.98	−6.89	22.09	−23.25	19.21	−4.04	1140049

Note: All the units are in kcal/mol. ΔE_{vdw} and ΔE_{ele} are the van der Waals and electrostatic contributions from MM. ΔG_{np} is the non-polar contribution to solvation and ΔG_p is the polar contribution to solvation. ΔG_{MM} is total gas-phase energy and ΔG_{sol} is total solvation energy. TΔS is entropic conformational change. ΔG_{pred} is calculated binding free energy by MM/GBSA method using the following equation: $\Delta G_{pred} = \Delta E_{MM}+\Delta G_{sol}$-(-TΔS); while ΔG_{exp} is experimental binding free energy derived from IC_{50} values calculated by the following equation: ΔG_{bind} = -RT ln(Ki_{cal}).

incorporation of entropy (-TΔS). The absolute ligand free energy of binding (ΔG_{bind}) with entropic contributions calculated through the amber-MMGBSA module and four energy components (ΔE_{vdw}, ΔE_{elec}, ΔG_p and ΔG_{np}) were carefully analyzed. From Table 3, it is evident that ΔE_{vdw} was dominant in all complexes and showed a value of -42.11 kcal/mol in AChE/**3a** and -40.26 kcal/mol in AChE/**3b**, likewise in BChE/**3a** (-39.88 kcal/mol) and BChE/**3b** (-37.19 kcal/mol) complexes. However, the ΔE_{elec} of AChE/**3a** complex (-16.2 kcal/mol) was found stronger compared to AChE/**3b** (-9.14 kcal/mol). In AChE/**3a**, the most representative conformation obtained from 20 ns MD clustering exhibited a more negative value of ΔE_{elec}, which was due to the network of consistent H-bonds interaction by the dinitrobenzene moiety in comparison to the presence of only H-bond in **3b**. The flipped orientation of **3b** due to the absence of dinitro group might contribute to less ΔE_{elec} towards overall ΔE_{bind}. A similar trend of energy contributions was observed by **3a** and **3b** with BChE. Overall, the energy contribution revealed a more favorable ΔG_{bind} (-14.13 kcal/mol) for **3a** as compared to **3b** (-8.32 kcal/mol) with AChE. While, values were found less negative in case of BChE/**3a** (-11.33 kcal/mol) and BChE/**3b** (-4.04 kcal/mol) (Table 3). The entropic contributions (-TΔS) which is the computationally most expensive calculations in MMGBSA method (Genheden and Ryde, 2015), revealed unfavorable for the ligands in all protein/ligand system. Furthermore, to estimate the rationale with the enzyme-based assay, measured inhibition constants (IC_{50}) of compounds were converted to experimental binding free energy (ΔG_{exp}), and the quantitative agreement was observed in **3a**/AChE between the calculated ΔG_{exp} and ΔG_{bind} as shown in Table 3.

The results of QikProp ADME predictions for **3a** and **3b** are presented in supplementary data (Table S1). Percentage oral absorption of 73 and 98 % were observed for **3a** and **3b**, respectively. Moreover, the values of blood brain permeability descriptors were observed well within the recommended limits of the QikProp manual.

4. Discussion

AD poses enormous social, health care and economic burden due to its time-dependent progression and ongoing treatment. On average, its annual treatment cost ranges from 12,000 to 19,000 USD, depending upon the type of drug regime (Mucha et al., 2008). Apart from the synthesis cost of the anti-AD drugs, bioavailability and specificity may also affect the amount of drug used and hence the overall cost. This accounts for a dire need for inexpensive drugs capable of lowering down the tremendous financial drain. This is only possible by the development of new drugs having high bioavailability and specificity, as well as, low synthesis cost.

The current study is an extension of our previously published work, where we used *in silico* tools to identify novel AChE inhibitors (Iman et al., 2018). Here, we report the synthesis and biological evaluation of two selected lead compounds (**3a** and **3b**). During our screening process, apart from promising *in silico* results, the economic feature was kept in mind. The ease of synthetic possibility and the cost-effective synthesis of these inhibitors using readily available substrates and short reaction scheme was taken into consideration. Chemically easy to synthesize small molecules involving high yield synthesis steps were selected for the synthesis, testing and development. As the number of steps increases in a multistep reaction scheme, the overall yield for the final product exponentially diminishes. The *bona fide* precept in the synthesis economy favors the decreased number of reactions steps in terms of cost and time, leading to the target molecule (Newhouse et al., 2009).

Different 2-naphthol, 3,5-dinitrobenzoic acids and 2-chloro-5-nitrobenzoic acid are among the readily available cheap starting materials required to synthesize selected compounds. The reaction schemes involved two steps and the yields of these steps were quantitative and therefore avoiding the need for lengthy and expensive purification steps, *e.g.*, chromatography. To the best of our knowledge, it is the first report of AChE, BChE, α-Glu and LOX inhibitory potential of these naphthalene derivatives connected to nitrobenzene residues *via* an ester linkage.

Due to the demonstration of excellent *in vitro* activity of **3a** against AChE, it was evaluated for *in vivo* potential in mice model. Acid hydrolysis on oral administration was a concern before the start of *in vivo* trial. However, plenty of evidence is available in literature in the form of salsalate, aspirin, remimazolam, propanidid, parabens, *etc.*, where aromatic and aliphatic esters are administrated orally. Alongside this, a large amount of data is available where closely related esters have been trialed in the animal models *via* oral route (Husain et al., 2012; Abbas et al., 2010; Masic et al., 2015). Highly nonpolar nature of the selected compounds and the presence of bulky aromatic residues could hinder the approach of water for hydrolysis and proton attach on ester moiety, thus, avoiding acid-induced ester hydrolysis. Moreover, QikProp from Schrödinger Suite is among the most reputed *in silico* tools for the ADME analysis, including oral stability, oral absorption and blood brain permeability. The QikProp predictions potentiated the hypothesis of oral administration of selected compounds with auspicious results. Since permeability is one of the most factors affecting drug absorption (Volpe, 2008), the predictive values obtained for **3a** displayed significant permeability using Caco-2 and MDCK cell permeability model (develop in QikProp), which signifies the optimum physicochemical properties necessary for a drug to cross the BBB (Jeffrey and Summerfield, 2010).

A selected dose of 5 mg/kg was orally administrated for seven days and brain tissues were examined for the concentration of AChE and photomicrographs. Both the test compounds presented a significant drop in AChE levels in brain tissue as compared to the control. Alongside this, no noticeable changes were observed among photomicrographs of brain tissues of different groups. Through molecular modeling, the binding pose of the most active compound **3a** observed after 20 ns MD simulation displayed good rationale with the enzyme inhibition assays, where the H-bonds established by nitro groups of **3a** might play a key role in AChE enzyme inhibition. Moreover, in AChE/**3a**, the observed π-π stacking interaction between the terminal dinitrobenzene moiety and Tyr337 was evident from a cation-π interaction between the piperidine ring of donepezil (Cheung et al., 2012), and this particular interaction was not observed with **3b**. Moreover, the role of Tyr337 is crucial for enzyme inhibition, as observed with the interaction of donepezil (Cheung et al., 2012) and huperzine A (Ashani et al., 1994) to the active site of human AChE. While binding at the active site, three additional H-bonds with Tyr341 and Asp74 could make the interaction stronger, which were found absent in complex with donepezil. Hence, the stability of the AChE/**3a** complex was evident due to vdW and electrostatic interaction and ligand did not undergo conformational changes during MD simulations. Therefore, **3a** displayed higher free energy of binding in comparison to **3b**.

Among four FDA approved cholinesterase inhibitors (galantamine, rivastigmine, tacrine, and donepezil) only donepezil can inhibit targets involved in inflammation including IL-1β (Reale et al., 2005; Zhang et al., 2015) and TSG-6 (Hwang et al., 2010). Yiran Wu *et. al.* (2012) has reported anti-inflammatory activity of naphthalen-1-yl 3,5-dinitrobenzoate with IC_{50} values of 1.04 and 8.6 μM against human 5-LOX in cell-free and human whole blood assays, respectively (Wu et al., 2012). This close analogy of compounds identified in this study with naphthalen-1-yl 3,5-dinitrobenzoate, having potent anti-inflammatory activity, intended towards LOX inhibitory potential of **3a** and **3b**. In this study, **3a** presented 45.26 % inhibition of LOX at 0.5 Mm while quercetin standard inhibited 89.25 % of the enzyme at the same concentration. So, the substitution of 3,5-dinitrobenzoate residue at 2-position of naphthalene (**3a**) resulted in around 50 % drop in the LOX inhibitory activity as compared to naphthalen-1-yl 3,5-dinitrobenzoate.

5. Conclusion

The study validates that the selected compounds could serve as multitargeting inhibitors for the control of AD. The percentage inhibitions of 89.13 and 63.27 % against AChE and BChE, respectively,

were observed with **3a** at 0.5 mM concentration. *In vivo* studies corroborated these observations with a considerable decrease in AChE levels in brain homogenates after the administration of **3a**. Consequently, it could serve as a potential candidate for future development as an anti-AD drug.

Authors contribution

Experimental work and data collection: Fareeha Anwar, Atta Ur Rehman and Uzma Saleem; design of the study: Bashir Ahmad, Sarfraz Ahmad; statistical analysis: Matheus Froeyen, Muhammad Usman Mirza and Nauman Mazhar; *in silico* analysis and interpretation of the data: Muhammad Ashraf: drafting the manuscript: critical revision of the manuscript: Sarfraz Ahmad, Lee Yean Kee and Iskandar Abdullah.

Declaration of Competing Interest

The authors report no declarations of interest.

Acknowledgments

The authors highly acknowledge Malaya University (grant no.: IIRG003A-2019) and Riphah International University (Lahore Campus) for dispensing necessary resources to conduct this work. We would especially like to thank Prof. Outi Salo-Ahen, Åbo Akademi University, Finland, for carrying out the QikProp property prediction (Schrödinger Release 2020-1: QikProp, Schrödinger, LLC, New York, NY, 2020.). Biocenter Finland Bioinformatics and Drug Discovery and Chemical Biology networks, CSC IT Center for Science, and Prof. Mark Johnson and Dr. Jukka Lehtonen are gratefully acknowledged for the excellent computational infrastructure at the Åbo Akademi University.

Appendix A. Supplementary data

Supplementary material related to this article can be found, in the online version, at doi:https://doi.org/10.1016/j.compbiolchem.2020.107378.

References

Abbas, S., Greige-Gerges, H., Karam, N., Piet, M.-H., Netter, P., Magdalou, J., 2010. Metabolism of parabens (4-hydroxybenzoic acid esters) by hepatic esterases and UDP-glucuronosyltransferases in man. Drug Metab. Pharmacokinet. 1009280069-1009280069.

Ashani, Y., Grunwald, J., Kronman, C., Velan, B., Shafferman, A., 1994. Role of tyrosine 337 in the binding of huperzine A to the active site of human acetylcholinesterase. Mol. Pharmacol. 45, 555–560.

Cao, Q., Jiang, K., Zhang, M., Liu, Y., Xiao, S., Zuo, C., Huang, H., 2003. Brain glucose metabolism and neuropsychological test in patients with mild cognitive impairment. Chinese Med. J. 116, 1235–1238.

Cheung, J., Rudolph, M.J., Burshteyn, F., Cassidy, M.S., Gary, E.N., Love, J., Franklin, M. C., Height, J.J., 2012. Structures of human acetylcholinesterase in complex with pharmacologically important ligands. J. Med. Chem. 55, 10282–10286.

Crespo-Biel, N., Theunis, C., Van Leuven, F., 2012. Protein tau: prime cause of synaptic and neuronal degeneration in Alzheimer's disease. Int. J. Alzheimers Dis. 2012.

De Felice, F.G., Ferreira, S.T., 2014. Inflammation, defective insulin signaling, and mitochondrial dysfunction as common molecular denominators connecting type 2 diabetes to Alzheimer disease. Diabetes 63, 2262–2272.

Desai, N., Shihora, P., Rajpara, K., Joshi, V., Vaghani, H., Satodiya, H., Dodiya, A., 2012. Synthesis, characterization, and antimicrobial evaluation of novel naphthalene-based 1, 2, 4-triazoles. Med. Chem. Res. 21, 2981–2989.

Di Francesco, A., Arosio, B., Gussago, C., Dainese, E., Mari, D., D'Addario, C., Maccarrone, M., 2013. Involvement of 5-lipoxygenase in Alzheimer's disease: a role for DNA methylation. J. Alzheimers Dis. 37, 3–8.

Dickson, M., Gagnon, J.P., 2009. The cost of new drug discovery and development. Discovery Med. 4, 172–179.

Genheden, S., Ryde, U., 2015. The MM/PBSA and MM/GBSA methods to estimate ligand-binding affinities. Expert Opin. Drug Discov. 10, 449–461.

Hebert, L.E., Scherr, P.A., Bienias, J.L., Bennett, D.A., Evans, D.A., 2003. Alzheimer disease in the US population: prevalence estimates using the 2000 census. Arch. Neurol. (60), 1119–1122.

Hira, S., Saleem, U., Anwar, F., Sohail, M.F., Raza, Z., Ahmad, B., 2019. β-Carotene: A natural compound improves cognitive impairment and oxidative stress in a mouse model of streptozotocin-induced Alzheimer's disease. Biomolecules 9, 441.

Hou, T., Wang, J., Li, Y., Wang, W.J.J.oci., 2011a. MOdeling. Assessing the Performance of the MM/PBSA and MM/GBSA Methods. 1. The Accuracy of Binding Free Energy Calculations Based on Molecular Dynamics Simulations, 51, pp. 69–82.

Hou, T., Wang, J., Li, Y., Wang, W., 2011b. Assessing the performance of the MM/PBSA and MM/GBSA methods. 1. The accuracy of binding free energy calculations based on molecular dynamics simulations. J. Chem. Inf. Model. 51, 69–82.

Hoyer, S., Lannert, H., 1999. Inhibition of the neuronal insulin receptor causes Alzheimer-like disturbances in oxidative/energy brain metabolism and in behavior in adult rats. Ann. N. Y. Acad. Sci. 893, 301–303.

Husain, S.S., Pejo, E., Ge, R., Raines, D.E., 2012. Modifying methoxycarbonyl etomidate's inter-ester spacer optimizes *in vitro* metabolic stability and *in vivo* hypnotic potency and duration of action. Anesthesiology 117, 1027.

Hwang, J., Hwang, H., Lee, H.-W., Suk, K., 2010. Microglia signaling as a target of donepezil. Neuropharmacology 58, 1122–1129.

Ikram, N., Mirza, M.U., Vanmeert, M., Froeyen, M., Salo-Ahen, O.M., Tahir, M., Qazi, A., Ahmad, S.J.B., 2019. Inhibition of oncogenic kinases: an *in vitro* validated computational approach identified potential multi-target anticancer compounds. Biomolecules 9, 124.

Iman, K., Mirza, M.U., Mazhar, N., Vanmeert, M., Irshad, I., Kamal, M.A., 2018. *In silico* structure-based identification of novel acetylcholinesterase inhibitors against Alzheimer's disease. CNS Neurol. Disord. Drug Targets 17, 54–68.

Jeffrey, P., Summerfield, S., 2010. Assessment of the blood–brain barrier in CNS drug discovery. Neurobiol. Dis. 37, 33–37.

Jia, J.-J., Zeng, X.-S., Song, X.-Q., Zhang, P.-P., Chen, L., 2017. Diabetes mellitus and Alzheimer's disease: the protection of epigallocatechin-3-gallate in streptozotocin injection-induced models. Front. Pharmacol. 8, 834.

Kang, H.M., Saltveit, M.E., 2002. Reduced chilling tolerance in elongating cucumber seedling radicles is related to their reduced antioxidant enzyme and DPPH-radical scavenging activity. Physiol. Plant. 115, 244–250.

Maier, J.A., Martinez, C., Kasavajhala, K., Wickstrom, L., Hauser, K.E., Simmerling, C., 2015. ff14SB: Improving the accuracy of protein side chain and backbone parameters from ff99SB. J. Chem. Theory Comput. 11, 3696–3713. https://doi.org/10.1021/acs.jctc.5b00255.

Masic, A., Hernandez, A.M.V., Hazra, S., Glaser, J., Holzgrabe, U., Hazra, B., Schurigt, U., 2015. Cinnamic acid bornyl ester derivatives from valeriana wallichii exhibit antileishmanial *in vivo* activity in leishmania major-infected balb/c mice. PLoS One 10.

Matsuoka, Y., Picciano, M., La Francois, J., Duff, K., 2001. Fibrillar β-amyloid evokes oxidative damage in a transgenic mouse model of Alzheimer's disease. Neuroscience 104, 609–613.

Mirza, M.U., Rafique, S., Ali, A., Munir, M., Ikram, N., Manan, A., Salo-Ahen, O.M., Idrees, M.J.Sr., 2016. Towards peptide vaccines against Zika virus: immunoinformatics combined with molecular dynamics simulations to predict antigenic epitopes of Zika viral proteins. Sci. Rep. 6, 37313.

Mirza, M.U., Vanmeert, M., Froeyen, M., Ali, A., Rafique, S., Idrees, M.J.Sr., 2019. *In silico* structural elucidation of RNA-dependent RNA polymerase towards the identification of potential Crimean-Congo hemorrhagic fever virus inhibitors. Sci. Rep. 9, 1–18.

Mucha, L., Wang, S.S., Cuffel, B., McRae, T., Mark, T.L., Valle, Md., 2008. Comparison of cholinesterase inhibitor utilization patterns and associated health care costs in Alzheimer's disease. J. Manag. Care Spec. Pharm. 14, 451–461.

Newhouse, T., Baran, P.S., Hoffmann, R.W., 2009. The economies of synthesis. Chem. Soc. Rev. 38, 3010–3021.

Noor, Z.I., Ahmed, D., Rehman, H.M., Qamar, M.T., Froeyen, M., Ahmad, S., Mirza, M.U. J.B., 2019. *In vitro* antidiabetic, anti-obesity and antioxidant analysis of *Ocimum basilicum* aerial biomass and *in silico* molecular docking simulations with alpha-amylase and lipase enzymes. Biology 8, 92.

Piazzi, L., Cavalli, A., Colizzi, F., Belluti, F., Bartolini, M., Mancini, F., Recanatini, M., Andrisano, V., Rampa, A., 2008. Multi-target-directed coumarin derivatives: hAChE and BACE1 inhibitors as potential anti-Alzheimer compounds. Bioorg. Med. Chem. Lett. 18, 423–426.

Polidori, M.C., Mecocci, P., 2002. Plasma susceptibility to free radical-induced antioxidant consumption and lipid peroxidation is increased in very old subjects with Alzheimer disease. J. Alzheimers Dis. 4, 517–522.

Qiu, C., Kivipelto, M., von Strauss, E., 2009. Epidemiology of Alzheimer's disease: occurrence, determinants, and strategies toward intervention. Dialogues Clin. Neurosci. 11, 111.

Rådmark, O., Werz, O., Steinhilber, D., Samuelsson, B., 2007. 5-Lipoxygenase: regulation of expression and enzyme activity. Trends Biochem. Sci. 32, 332–341.

Reale, M., Iarlori, C., Gambi, F., Lucci, I., Salvatore, M., Gambi, D., 2005. Acetylcholinesterase inhibitors effects on oncostatin-M, interleukin-1β and interleukin-6 release from lymphocytes of Alzheimer's disease patients. Exp. Gerontol. 40, 165–171.

Riaz, S., Khan, I.U., Bajda, M., Ashraf, M., Shaukat, A., Rehman, T.U., Mutahir, S., Hussain, S., Mustafa, G., Yar, M., 2015. Pyridine sulfonamide as a small key organic molecule for the potential treatment of type-II diabetes mellitus and alzheimer's disease: in vitro studies against yeast α-glucosidase, acetylcholinesterase and butyrylcholinesterase. Bioorg. Chem. 63, 64–71.

Rojas-Gutierrez, E., Muñoz-Arenas, G., Treviño, S., Espinosa, B., Chavez, R., Rojas, K., Flores, G., Díaz, A., Guevara, J., 2017. Alzheimer's disease and metabolic syndrome: a link from oxidative stress and inflammation to neurodegeneration. Synapse 71, e21990.

Saleem, F., Mehmood, R., Mehar, S., Khan, M.T.J., Khan, Z.-u.-D., Ashraf, M., Ali, M.S., Abdullah, I., Froeyen, M., Mirza, M.U.J.A., 2019. Bioassay directed isolation, biological evaluation and *in* silico studies of new isolates from *Pteris cretica* L. Antioxidants 8, 231.

Sugaya, K., Uz, T., Kumar, V., Manev, H., 2000. New anti-inflammatory treatment strategy in Alzheimer's disease. Japanese J. Pharmacol. 82, 85–94.
Sun, H., Li, Y., Tian, S., Xu, L., Hou, T., 2014. Assessing the performance of MM/PBSA and MM/GBSA methods. 4. Accuracies of MM/PBSA and MM/GBSA methodologies evaluated by various simulation protocols using PDBbind data set. Phys. Chem. Chem. Phys. 16, 16719–16729.
Trott, O., Olson, A.J., 2010. AutoDock Vina: improving the speed and accuracy of docking with a new scoring function, efficient optimization, and multithreading. J. Comput. Chem. 31, 455–461.
Volpe, D.A., 2008. Variability in Caco-2 and MDCK cell-based intestinal permeability assays. J. Pharm. Sci. 97, 712–725.
World Health Organization, 2019. New Guide for Carers of People with Dementia [Internet]. [cited 2020 Feb 29]. http://who.int/mental_health/neurology/dementia.
Wu, Y., He, C., Gao, Y., He, S., Liu, Y., Lai, L., 2012. Dynamic modeling of human 5-lipoxygenase–inhibitor interactions helps to discover novel inhibitors. J. Med. Chem. 55, 2597–2605.
Xu, L., Sun, H., Li, Y., Wang, J., Hou, T., 2013. Assessing the performance of MM/PBSA and MM/GBSA methods. 3. The impact of force fields and ligand charge models. J. Phys. Chem. B 117, 8408–8421.
Yar, M., Bajda, M., Atif Mehmood, R., Rukh Sidra, L., Ullah, N., Shahzadi, L., Ashraf, M., Ismail, T., Anjum Shahzad, S., Ali Khan, Z., 2014a. Design and synthesis of new dual binding site cholinesterase inhibitors: *in vitro* inhibition studies with *in silico* docking. Lett. Drug Des. Discov. 11, 331–338.
Yar, M., Sidra, L.R., Pontiki, E., Mushtaq, N., Ashraf, M., Nasar, R., Khan, I.U., Mahmood, N., Naqvi, S.A.R., Khan, Z.A., 2014b. Synthesis, in vitro lipoxygenase inhibition, docking study and thermal stability analyses of novel indole derivatives. J. Iranian Chem. Soci. 11, 369–378.
Zhang, T., Tian, F., Wang, J., Zhou, S., Dong, X., Guo, K., Jing, J., Zhou, Y., Chen, Y., 2015. Donepezil attenuates high glucose-accelerated senescence in human umbilical vein endothelial cells through SIRT1 activation. Cell Stress Chaperones 20, 787–792.